The Mechanical Stability of Austenite and Cryogenic Toughness of Ferritic Fe-Mn-Al Alloys

SANG WOO LEE and HU-CHUL LEE

In an attempt to understand the role of retained austenite on the cryogenic toughness of a ferritic Fe-Mn-Al steel, the mechanical stability of austenite during cold rolling at room temperature and tensile deformation at ambient and liquid nitrogen temperature was investigated, and the microstructure of strain-induced transformation products was observed by transmission electron microscopy (TEM). The volume fraction of austenite increased with increasing tempering time and reached 54 pct after 650 °C, 1-hour tempering and 36 pct after 550 °C, 16-hour tempering. Saturation Charpy impact values at liquid nitrogen temperature were increased with decreasing tempering temperature, from 105 J after 650 °C tempering to 220 J after 550 °C tempering. The room-temperature stability of austenite varied significantly according to the ($\alpha + \gamma$) region tempering temperature; *i.e.*, in 650 °C tempered specimens, 80 to 90 pct of austenite were transformed to lath martensite, while in 550 °C tempered specimens, austenite remained untransformed after 50 pct cold reductions. After tensile fracture (35 pct tensile strain) at −196 °C, no retained austenite was observed in 650 °C tempered specimens, while 16 pct of austenite and 6 pct of ϵ-martensite were observed in 550 °C tempered specimens. Considering the high volume fractions and high mechanical stability of austenite, the crack blunting model seems highly applicable for improved cryogenic toughness in 550 °C tempered steel. Other possible toughening mechanisms were also discussed.

I. INTRODUCTION

FERRITIC steels have advantages of lower cost and higher strength for cryogenic application when compared to austenitic steels. But ferritic steels undergo ductile–brittle transition at lower temperatures, and for structural application, the ductile–brittle transition temperature (DBTT) must be suppressed to below the intended service temperature. In 5 to 12 Ni steels,[1–5] successful metallurgical processes have been developed to lower the DBTT to below liquid nitrogen temperature, and these steels were extensively used for liquefied natural gas storage tank application. These metallurgical processes include repeated heating to the γ and upper ($\alpha + \gamma$) region followed by final tempering at the lower ($\alpha + \gamma$) region. Thermal cycling in the γ and ($\alpha + \gamma$) region was known to be an effective way to reduce the grain size, and final tempering at the lower ($\alpha + \gamma$) region was essential to suppress the DBTT to below −196 °C. Small volume fractions of fine austenite were precipitated in interlath or prior austenite grain boundaries during this final tempering. The beneficial effects of these fine austenite particles on cryogenic toughness are well recognized by many researchers, but the mechanism of toughening is not well understood yet and still remains a controversial research topic.

Application of identical thermal processing technique to Fe-Mn steel was not very successful mainly because[6,7,8] (1) nickel increases the stacking fault energy of iron to assist the cross slip of screw dislocation while manganese reduces the stacking fault energy to enhance the cleavage fracture, and (2) when Mn contents exceed 8 pct, hexagonal ϵ-martensite precipitates to interrupt the grain refining by thermal cycling. Despite these difficulties, substitution of nickel by manganese has a substantial advantage of lowering production costs, which provides sufficient incentives to develop nickel-free ferritic cryogenic steel. Niikura and Morris[9] achieved a good combination of strength and toughness at −196 °C in Fe-5Mn steel. In this steel, the manganese content was limited to prevent the intrusion of ϵ-martensite during thermal treatment. It is also expected that, if the precipitation of ϵ-martensite could be suppressed by the addition of a third alloying element, higher manganese steels should be processed by a similar method.

In our previous article,[10] we reported that the addition of aluminum could effectively prevent the precipitation of ϵ-martensite in 12 to 13 pct Mn steel, and Fe-13Mn-3Al steel was successfully processed to produce good impact toughness at liquid nitrogen temperature. The critical thermal process for good cryogenic toughness was also known to be the final tempering treatment at the lower ($\alpha + \gamma$) region. But the amount of retained austenite after tempering treatment was relatively large in this steel compared to 9Ni steel, and the role of austenite in toughening this steel at cryogenic temperature might differ from that of austenite in 9Ni steel.

In this study, the mechanical stability of austenite precipitated during final tempering was evaluated by mechanical rolling at room temperature and by tensile tests at room and liquid nitrogen temperatures. The relationships between the mechanical stability of austenite and Charpy impact toughness at −196 °C were discussed.

II. EXPERIMENTAL PROCEDURE

A 15-kg ingot of nominal Fe-13Mn-3Al alloy was vacuum induction melted and cast into a cast iron mold.

SANG WOO LEE, formerly Graduate Student, Seoul National University, is Research Scientist, Research Institute of Industrial Science and Technology, Pohang, Kyungsangbuk-Do 790-600, Korea. HU-CHUL LEE, Professor, is with the Department of Metallurgical Engineering and Center for Advanced Materials Research, Seoul National University, Kwanak-Ku, Seoul 151-742, Korea.

Manuscript submitted June 5, 1992.

Table I. Chemical Composition of Fe-Mn-Al Alloy (Weight Percent)

C	Si	Mn	Al	Mo	P	S	Fe
0.005	0.07	12.7	2.73	0.31	0.002	0.003	Bal.

The ingot was homogenized at 1200 °C for 24 hours and then forged and hot rolled to a 13-mm-thick flat plate. Drill chips were randomly collected from the rolled plate and chemically analyzed. The result of chemical analysis is given in Table I. Specimen blanks were cut from the hot-rolled plate and subjected to ($\alpha + \gamma$) and γ cycling heat treatment for grain refining. Temperatures of 760 °C and 840 °C were chosen for ($\alpha + \gamma$) and γ cycling heat treatment, and the cycling was repeated twice. Final tempering treatments were conducted at 550 °C, 600 °C, and 650 °C for 1/4 to 64 hours depending on tempering temperature. The heat-treatment procedure is sketched in Figure 1. Charpy impact specimens were machined from heat-treated blanks and tested at −196 °C according to ASTM standard. The fracture surfaces of broken Charpy impact specimens were observed using a JEOL JSM35 scanning electron microscope.

Mechanical stability of austenite precipitated during tempering treatment was investigated at room and liquid nitrogen temperatures by cold rolling and tensile deformation. At room temperature, tempered plates were rolled with the reduction ratio of 10, 20, 30, 40, and 50 pct.

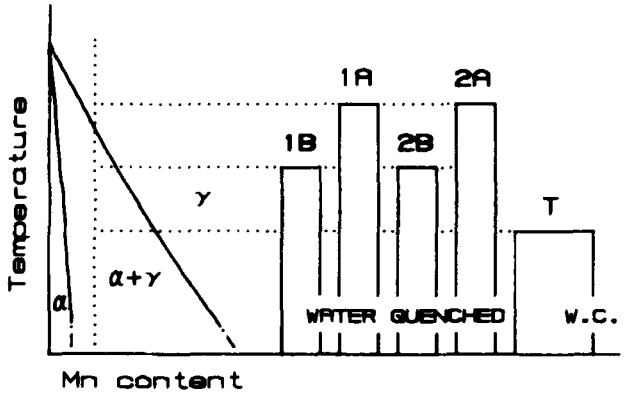

Fig. 1 — Schematic diagram for heat treatments.

Tensile specimens were cut along the hot rolling direction and tested to fracture at room and liquid nitrogen temperatures. Volume fractions of austenite and ε-martensite phase after ($\alpha + \gamma$) tempering and after rolling and tensile deformation were measured by an X-ray diffraction technique. Average integrated intensities of $(200)\alpha$, $(200)\gamma$, and $(1011)\varepsilon$ peaks by CuKα diffraction and $(200)\alpha$, $(220)\gamma$, $(211)\alpha$, and $(311)\gamma$ peaks by MoKα diffraction were compared. Samples were cut from several orientations to minimize the effect of preferred orientation.

For transmission electron microscopy (TEM), thin foils were prepared by a conventional twin-jet polishing technique using a 10 pct perchloric acid + 90 pct acetic acid solution. Perforated thin foils were investigated using a JEOL 200CX transmission electron microscope.

III. EXPERIMENTAL RESULTS

A. *Microstructure*

Figure 2 shows the optical micrographs of heat-treated plates. After hot rolling at 900 °C, the 13-mm-thick slab was air cooled to room temperature, and a full martensite structure was developed during air cooling (Figure 2(a)). Lath structures are not clearly visible in this as-quenched martensite. After repeating ($\alpha + \gamma$) and γ cycles, grain refinement was achieved in some degree (Figure 2(b)), but the refinement was not as significant as observed in 9Ni or 12Ni steels. After lower ($\alpha + \gamma$) region tempering, lath structures were revealed (Figure 2(c)), probably due to the precipitation of austenite at lath boundaries.

The transmission electron micrographs of Fe-13Mn-3Al alloy after tempering at the lower ($\alpha + \gamma$) region are shown in Figure 3. By lower ($\alpha + \gamma$) region tempering, austenite particles were precipitated at lath boundaries. The orientations of austenite particles were identical within a lath packet. The size of austenite particles tends to increase with increased tempering temperature. Precipitation of ε-martensite within the austenite phase was observed after tempering, and the amount of ε-martensite also increased with increasing tempering temperature. Dilution of carbon and aluminum in the austenite phase is believed to be responsible for this behavior. In Figure 4, ε-martensite precipitated in austenite after 650 °C tempering is revealed by a $(1100)\varepsilon$ dark-field image. The orientation relationship between

Fig. 2 — Optical micrographs of Fe-13Mn-3Al alloy: (*a*) as-rolled, (*b*) ($\alpha + \gamma$) and γ cycled, and (*c*) lower ($\alpha + \gamma$) region tempered.

austenite and ε-martensite phases satisfied that of Shoji-Nishiyama,[11] *i.e.*, $[101]\gamma//[1120]\varepsilon$, $(111)\gamma//(0001)\varepsilon$. Many stacking faults associated with $a/6[121]$-type Shockley partial dislocations were also observed in austenite phase after 650 °C tempering.

B. *Volume Fraction of Austenite*

Figure 5 shows the variations in volume fraction of austenite and ϵ-martensite precipitated after (α + γ) region tempering and cooling into liquid nitrogen. The amount of precipitated austenite increased with tempering time and reached saturation to 52 pct after 650 °C, 1-hour tempering, to 44 pct after 600 °C, 4-hour tempering, and to 36 pct after 550 °C, 16-hour tempering. The ε-martensite was not observed in as-quenched martensite, but about 6 pct of ε-martensite were precipitated after 650 °C tempering. The ε-martensite was rarely observed in 550 °C tempered specimens.

C. *Charpy Impact Energy at −196 °C*

The Charpy impact energy of Fe-13Mn-3Al steel at −196 °C after (α + γ) region tempering is shown in Figure 6. The impact toughness increased with increasing tempering time, *i.e.*, with increasing amount of austenite, and reached maximum when the austenite fraction reached saturation. This dependence of impact values on austenite fraction strongly suggests direct effect of austenite on the cryogenic toughness of this steel. Nevertheless, when the effect of tempering temperature on the cryogenic toughness is considered, the role of austenite fraction seems reversed. Maximum impact values increased with decreasing tempering temperature, *i.e.*, with decreasing austenite volume fraction, and reached 220 J after tempering at 550 °C for longer than 16 hours.

The mechanical stability of austenite is believed to play a critical role in this tempering temperature dependence of cryogenic toughness, and an investigation of the mechanical stability of austenite was conducted. Figure 7 shows the fracture surface of broken Charpy specimens. Dimple fracture is the dominant fracture mode in 550 °C tempered specimens, but quasi-cleavage-like flat fracture areas (arrows) are often noticed in 650 °C tempered specimens.

D. *Mechanical Stability of Austenite at Room Temperature*

The strain-induced transformation of retained austenite in lower (α + γ) region tempered specimens was investigated by rolling at room temperature, and the amount of austenite after cold rolling is plotted in Figure 8 as a function of rolling reductions. The strain-induced transformation was minimized in 550 °C tempered specimens, and about three quarters of the tempered austenite survived a 50 pct rolling reduction. In 650 °C tempered specimens, the austenite volume fractions decreased to about half after 20 pct reduction and further decreased to about 10 pct by 50 pct cold reduction.

In Figures 9 and 10, the TEM micrographs of 550 °C and 600 °C tempered specimens after 50 pct rolling reduction are shown. Most of the austenite particles in 550 °C tempered specimens are deformed and contain

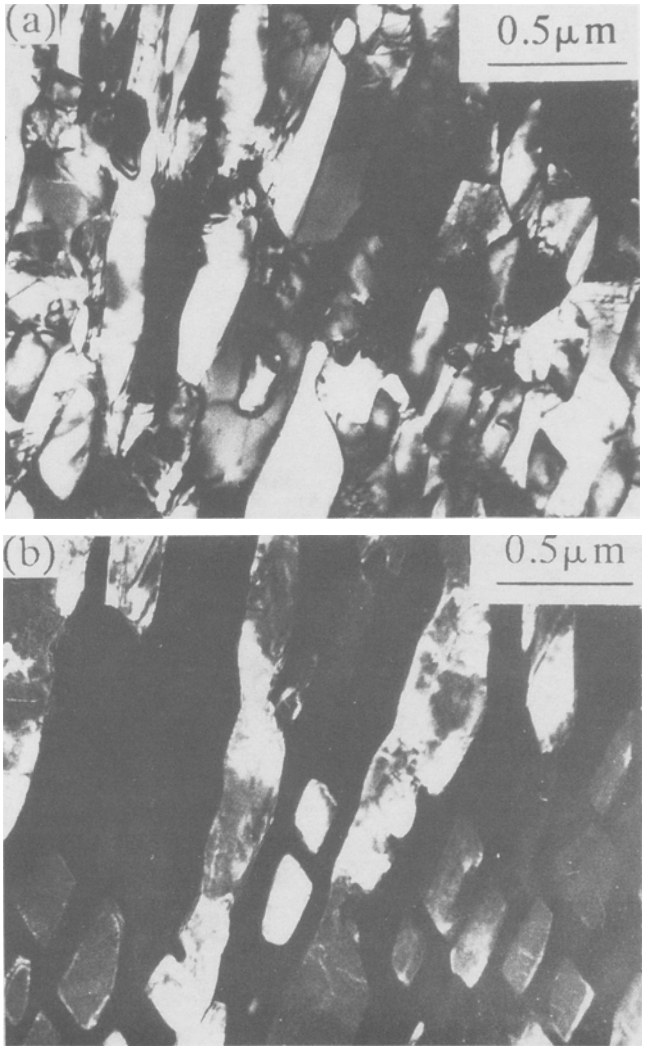

Fig. 3—TEM micrographs of Fe-13Mn-3Al alloy tempered at 600 °C for 4 h following cyclic heat treatment: (*a*) bright-field image and (*b*) dark-field image of retained austenite by (200)γ reflection.

many defects which are believed to be stacking faults, as demonstrated by streaking in the diffraction pattern, but rarely transformed to ε- or α'-martensites. In 600 °C tempered specimens, partial transformation of austenite to ε- and α'-martensite was frequently observed. Figure 11 shows the microstructure of 650 °C, 1-hour tempered specimens after a 10 pct rolling reduction. Strain-induced transformation to α'-martensite is revealed by $(011)\alpha'$ dark-field microscopy. The formation of α'-martensite is apparently associated with ε-martensites, which suggests a γ-ε-α' transformation path. Transformation of austenite to α'-martensite further progressed after 50 pct rolling reduction, as shown in Figure 12. ε-martensite was rarely observed. The diffraction pattern shows that the orientation of deformation-transformed α' is different from that of the matrix α phase. Kim *et al.*[5,12] had reported that the martensite variant adopted by the mechanically transformed austenite was usually different from the dominant variant of the surrounding martensite laths. It is believed that the orientations of mechanically transformed martensite were

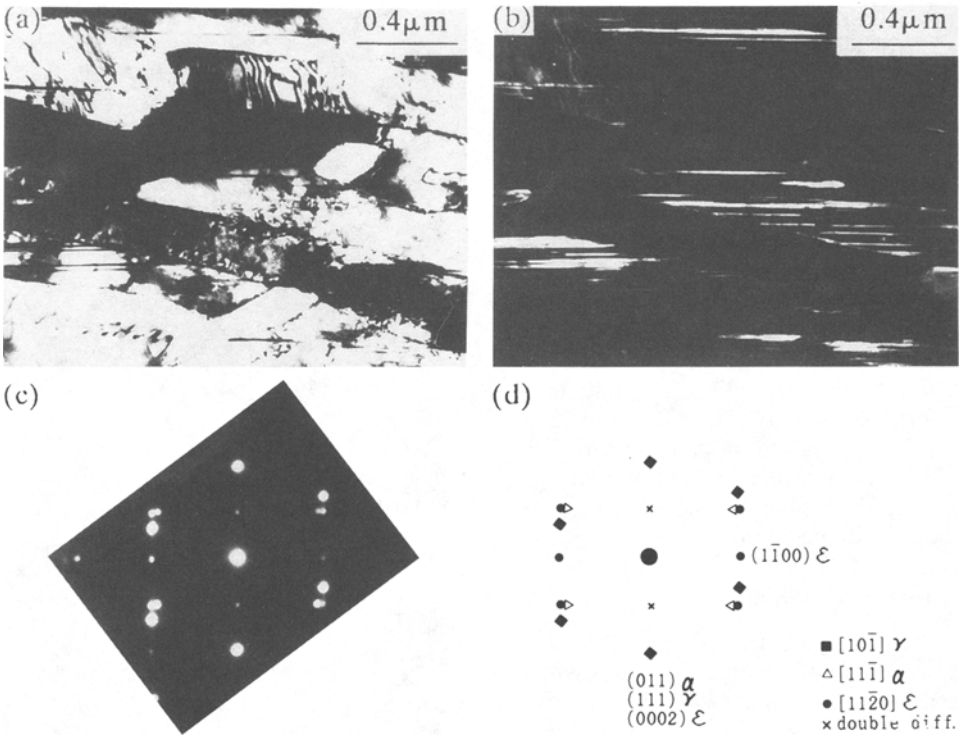

Fig. 4—TEM micrographs of ε-martensite precipitated in austenite phase after 650 °C tempering: (*a*) bright-field image, (*b*) dark-field image of ε-martensite by (1$\bar{1}$00)ε reflection, (*c*) selected area diffraction pattern from (ε + γ) grain, and (*d*) index of (*c*).

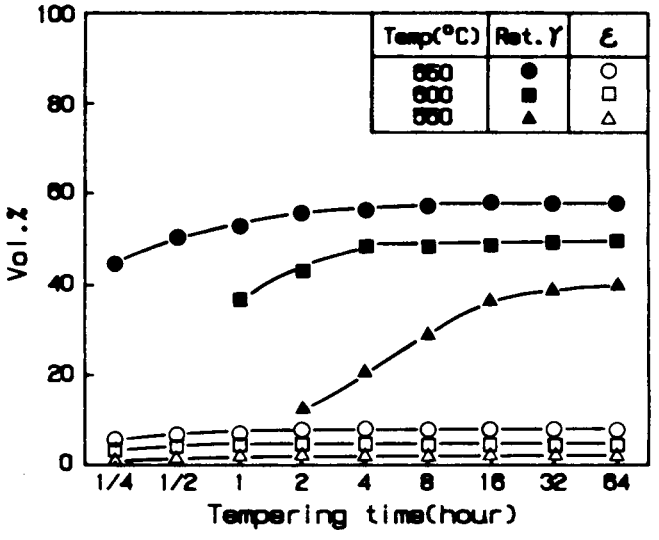

Fig. 5—Volume fraction of austenite and ε-martensite phase after tempering and cooling to liquid nitrogen temperature.

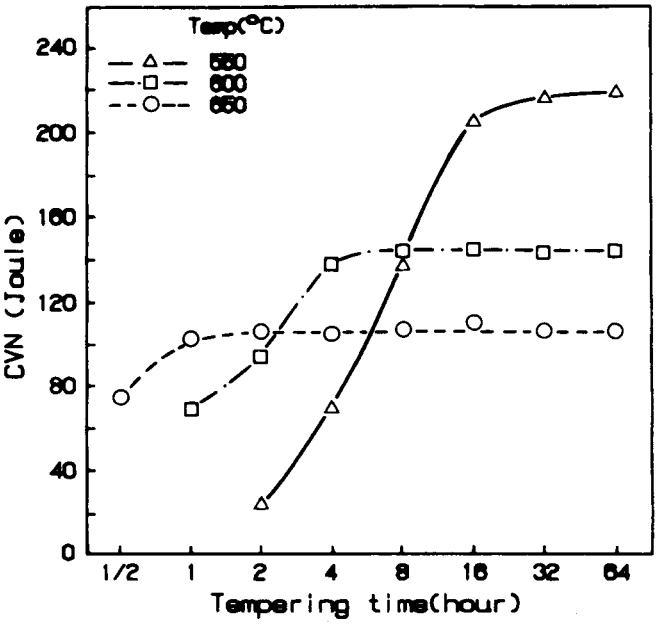

Fig. 6—Charpy impact energy of Fe-13Mn-3Al alloy as a function of tempering temperature and time (test temperature, −196 °C).

determined to accommodate the applied strain during deformation. Present observation confirms these observations despite the differences in transformation path in Fe-Ni and Fe-Mn alloys.

E. *Mechanical Stability of Austenite at −196 °C*

To investigate the mechanical stability of precipitated austenite at liquid nitrogen temperature, tensile tests were carried out in liquid nitrogen. After tensile fracture, volume fractions of austenite and ε-martensite were measured by X-ray method and are listed in Table II. Data from room-temperature tests are also given for comparison.

Complete transformation of austenite and ε-martensite to α′-martensite was observed in 650 °C tempered specimens, while partial transformation to α′- or ε-martensite occurred in 550 °C tempered specimens. In Figure 13, ε-martensite precipitated during tensile deformation of 550 °C tempered specimens was revealed

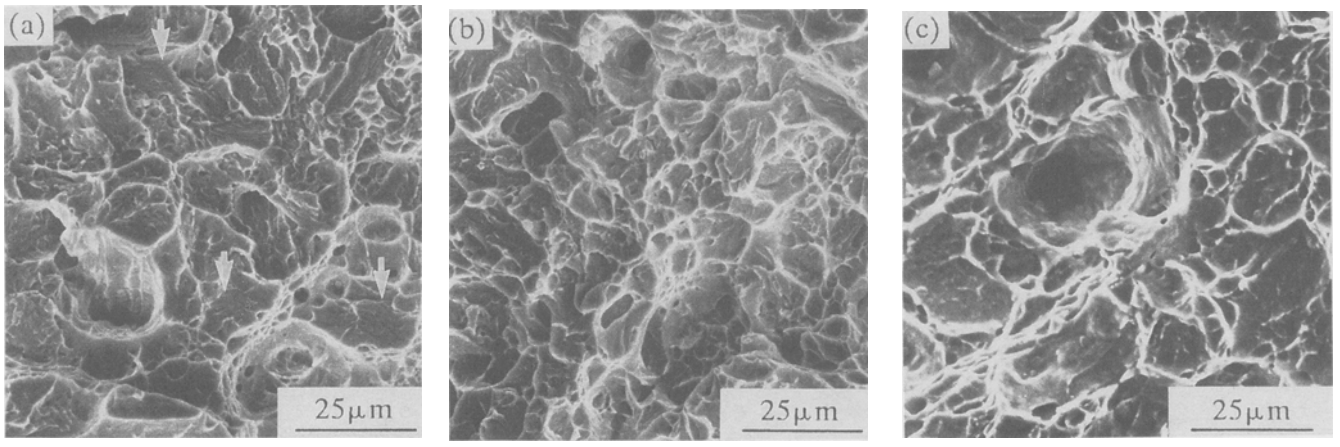

Fig. 7—Scanning electron micrographs of fracture surfaces of Charpy specimens broken at −196 °C. Specimens were cyclic heat-treated and tempered at (*a*) 650 °C for 1 h, (*b*) 600 °C for 4 h, and (*c*) 550 °C for 16 h.

by $(1\bar{1}00)\varepsilon$ dark-field electron microscopy. Figure 14 shows the TEM micrograph of 650 °C tempered specimens after tensile deformation to fracture. Precipitated austenite particles were all transformed to fine dislocated martensites. The diffraction pattern from these martensites shows that these fine martensites are twin related to each other. This type of twin-related martensite is known to form in austenite of low stacking fault energy[13] and has a lattice invariant shear of $(111)\gamma[\bar{1}2\bar{1}]\gamma$ type, as predicted by Bowles and Mackenzie,[14] instead of the $(110)\gamma[1\bar{1}0]\gamma$ system used to account for the more familiar transformation to internally twinned martensite.

IV. DISCUSSION

A. *Mechanical Stability of Austenite*

As demonstrated in Figure 8, the differences in the mechanical stability of austenite precipitated during the tempering process are remarkable. In 650 °C tempered specimens, stacking faults and ε-martensite were readily developed after 10 pct cold reduction, and α'-martensite was formed within or accompanied by ε-martensite plates. After 50 pct reduction at room temperature, more than 90 pct of precipitated austenite phase was transformed to ε-martensite or α'-martensite. In 600 °C tempered specimens, only partial transformation to α'-martensite occurred after 50 pct cold reduction, and the microstructure looked quite similar to that of 650 °C tempered specimens after 10 pct cold reduction. The mechanical stability of 550 °C tempered austenite was quite excellent. Only less than a quarter of precipitated austenite was transformed to ε-martensite or α'-martensite even after 50 pct cold reduction at room temperature, and many stacking faults and dislocations were observed in untransformed austenite.

It was reported[15–19] that, in austenite with low stacking fault energy, transformation to α'-martensite occurs *via* the γ-ε-α' or γ-α' transformation path, while direct γ-to-α'-martensite transformation occurs in austenites with high stacking fault energy. The ε phase was considered to form by the superposition of stacking faults and was known to provide preferred nucleation sites for α'-martensite,[17,18,19] although the mechanism of superposition is not well understood. Manganese is a well-known element to decrease the stacking fault energy of austenite in Fe-Mn alloys, and when added above 10 wt pct, ε-martensite starts to form. Schumann[20] reported maximum precipitation of 50 pct ε-martensite in Fe-17 pct Mn alloys. Lysak *et al.*[21] also reported maximum precipitation of ε-martensite with a maximum number of stacking faults in the austenite at a manganese concentration of 14 to 15 pct. These results strongly suggest the minimum stacking fault energy of Fe-Mn austenite at a 15 to 17 pct manganese content. The stacking fault energy of Fe-Mn austenite was reported to rapidly increase with further addition of manganese.

Addition of aluminum to Fe-Mn alloys increases the stacking fault energy of austenite and suppresses the precipitation of ε-martensite.[10] In Fe-13Mn alloy, the precipitation of ε-martensite in quenched specimens decreased with increases in aluminum content and was fully suppressed when aluminum content exceeded 2 wt pct. Quenching after tempering at 650 °C resulted in numerous precipitation of ε-martensite in austenite particles, as shown in Figure 4. The increases in ε-martensite content in tempered specimens can be ascribed to the enrichment of manganese as well as the depletion of aluminum in the austenite phase during $(\alpha + \gamma)$ tempering. This redistribution of alloying elements will reduce the stacking fault energy of the precipitated austenite phase.

If the tempering temperature is reduced, more enrichment of manganese in the austenite phase is expected with the decrease in the amount of the austenite phase. The stacking fault energy of Fe-Mn austenite with Mn content higher than 17 pct should increase with increasing Mn content. Reduced precipitation of ε-martensite in 600 °C and 550 °C tempered specimens agrees with these expectations.

The mechanical stability of austenite precipitated in tempered steel could well be explained by the stacking fault energy of austenite. In 650 °C tempered steel, the stacking fault energy of austenite is lowest and the ε phase is already present in significant volume fractions. This ε phase could act as nucleation sites for α'-martensite, thus reducing the stability of austenite. In 550 °C tempered steel, the stacking fault energy of austenite is higher,

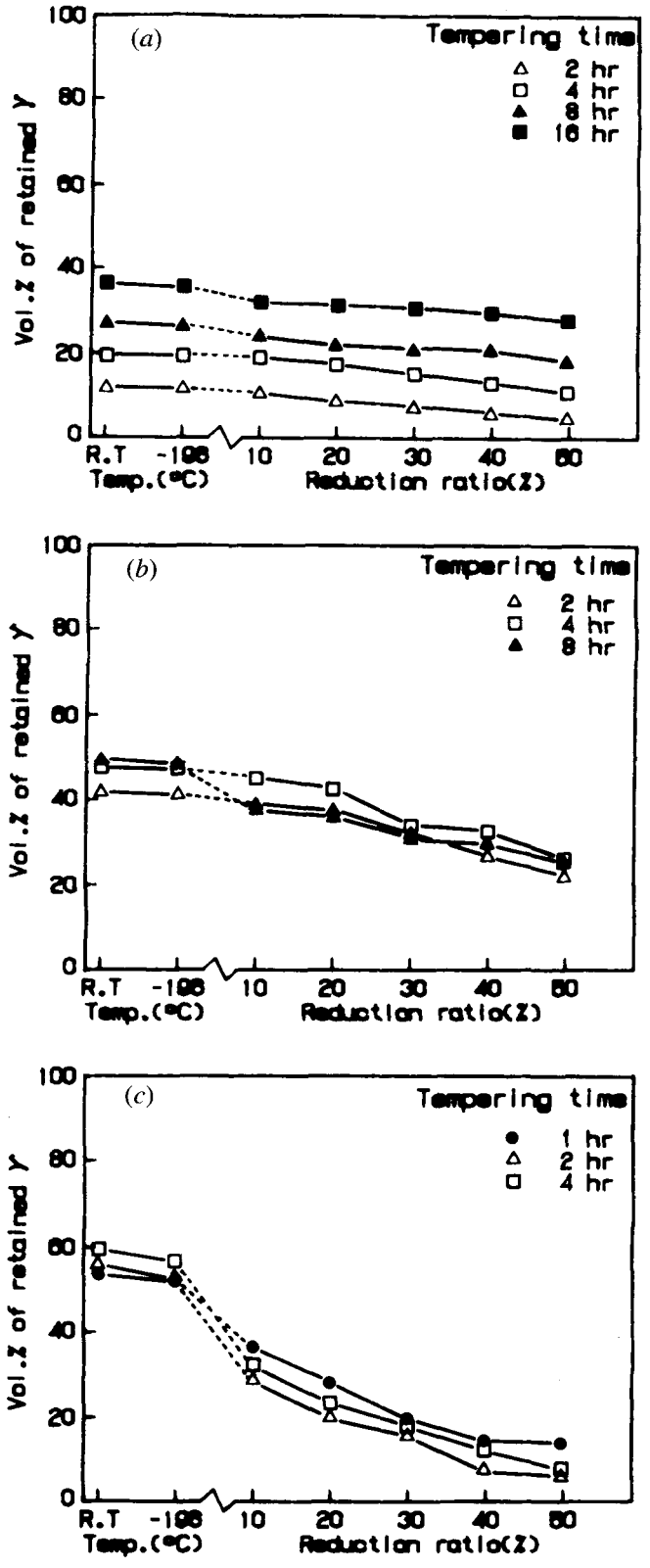

Fig. 8—Variations in austenite volume fractions with rolling at ambient temperature in specimens tempered at (*a*) 550 °C, (*b*) 600 °C, and (*c*) 650 °C.

and ε-martensite was rarely observed in tempered specimens. This austenite of high stacking fault energy does not readily transform to the ε or α′ phase and is mechanically more stable than higher temperature tempered austenite.

The stacking fault energy of austenite also decreases with decreasing temperature,[22,23] as does the mechanical stability of austenite. The results from the tensile deformation at liquid nitrogen temperature are consistent with the above statement. Complete transformation of austenite to α′-martensite occurred in 650 °C tempered specimens, and the transformation produced twin-related fine dislocated martensites. This type of martensite was reported[13,14] to form from a low stacking fault energy austenite. In 550 °C tempered steel, ε-martensites were often observed after tensile deformation at −196 °C, but about one half of the austenite survived the deformation near to fracture. Reduced but higher stacking fault energy of austenite in 550 °C tempered specimens than higher temperature tempered ones could be the explanation for this transformation behavior at liquid nitrogen temperature.

B. *The Role of Precipitated Austenite in the Cryogenic Toughness*

It is now well agreed that precipitation of a small volume fraction of thermally stable austenite during lower (α + γ) region tempering is beneficial to lowering the DBTT in ferritic cryogenic steel. However, the mechanism of toughening by retained austenite still remains somewhat unclear. Early explanations that ductile austenite toughens the steel by blunting the propagating cracks[24,25,26] were seriously questioned by later researchers, who found that these thermally stable austenites are mechanically unstable and transform to martensite in the plastic zone ahead of the crack tip. Kim and Schwartz[27] and Fultz and Morris[28] reported that an almost complete transformation of austenite occurred near the fracture surface of 9Ni steel specimens broken above the DBTT. Syn *et al.*[12] also studied the behavior of thermally stable austenite in the ductile fracture surface layer of 9Ni steel broken at −196 °C using Mossbauer spectroscopy and TEM. They reported that thermally stable austenite was mechanically unstable and transformed to dislocated martensite in the deformed zone adjacent to the ductile fracture surface. They concluded that transformation of austenite is compatible with low-temperature toughness as long as the transformation product is the ductile martensite. This claim by Syn *et al.* was later supplemented by Kim *et al.*[5] and Frear and Morris,[29] who observed that the crystallographic variants of the martensite formed during plastic deformation associated with the propagating crack usually differed from the common variant of the surrounding packets; hence, the cooperative cleavages within the martensite packet were impaired by these transformed martensites of new variants.

Research on thermally stable austenite in 6–9Ni steel dominantly supports the observation of complete transformation of austenite particles in the plastically deformed region near the crack tip. The key role of austenite

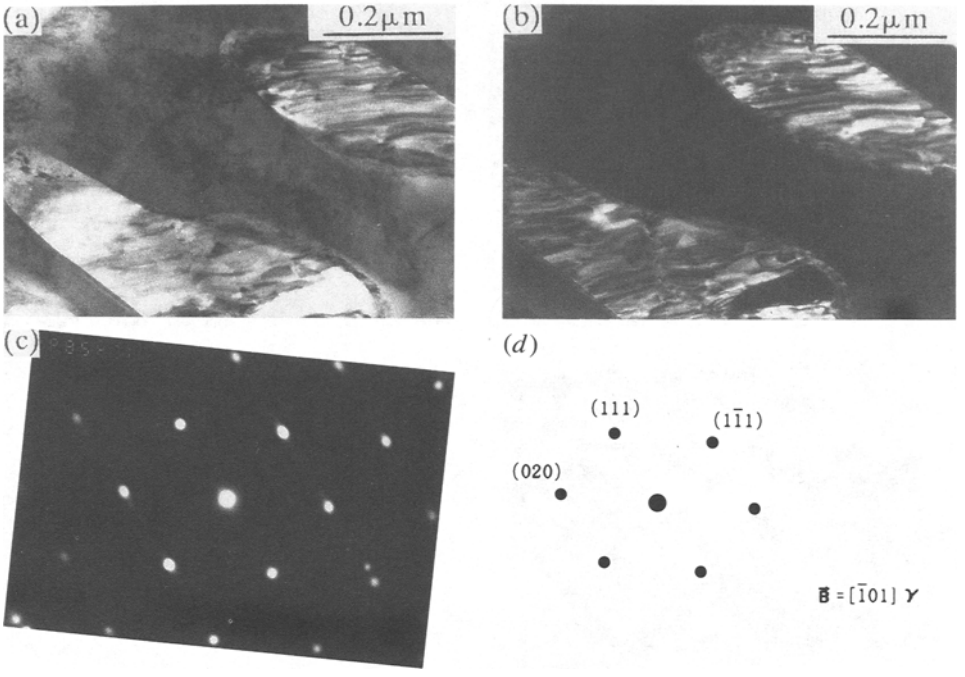

Fig. 9—Deformed austenite in 550 °C, 16-h tempered specimen after 50 pct cold reduction: (*a*) bright-field image, (*b*) (020)γ dark-field image, (*c*) selected area diffraction pattern, and (*d*) index of (*c*).

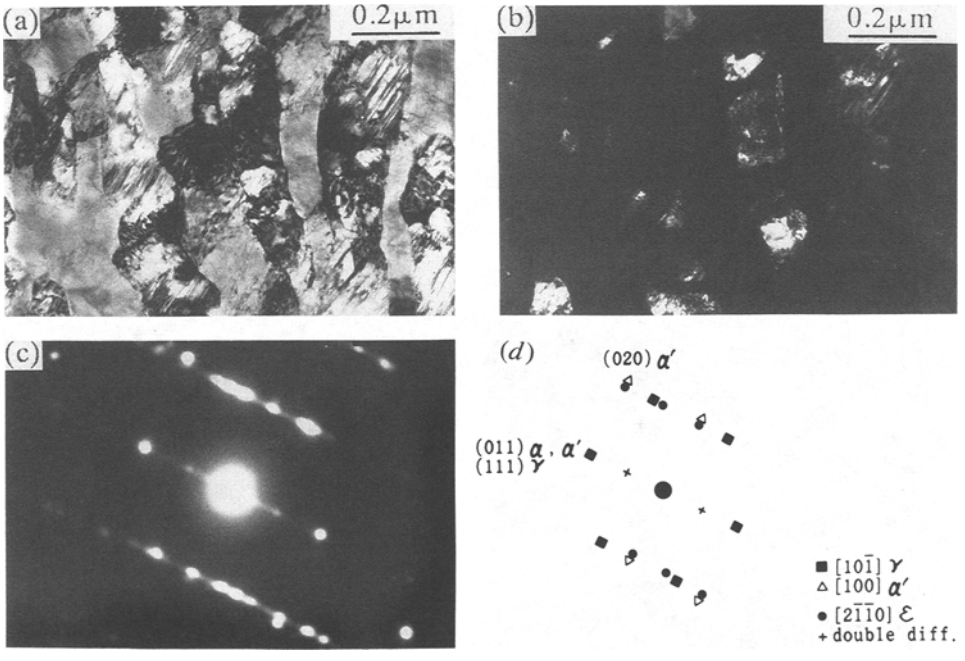

Fig. 10—Partially transformed austenite in 600 °C, 4-h tempered specimen after 50 pct cold reduction: (*a*) bright-field image, (*b*) (020)α′ dark-field image, (*c*) selected area diffraction pattern, and (*d*) index of (*c*).

in cryogenic toughness seems to be not whether it transforms during the impact test but, rather, how the transformation affects the crack propagation during the Charpy test.

Fultz and co-workers[28,30] tried to correlate the effects of the mechanical stability of austenite precipitated during tempering at 590 °C from 0.8 to 650 hours to Charpy impact values of 9Ni steel. The Charpy toughness correlated better with the stability of austenite than with the amount of austenite in the specimen. They observed many qualitative similarities in the dislocation structures around transformed large unstable austenite particles to the dislocation structure of cold-worked materials. This type of extensive microstructural damage around transformed large particles can promote brittle behavior. Meanwhile, the transformation of small stable austenite

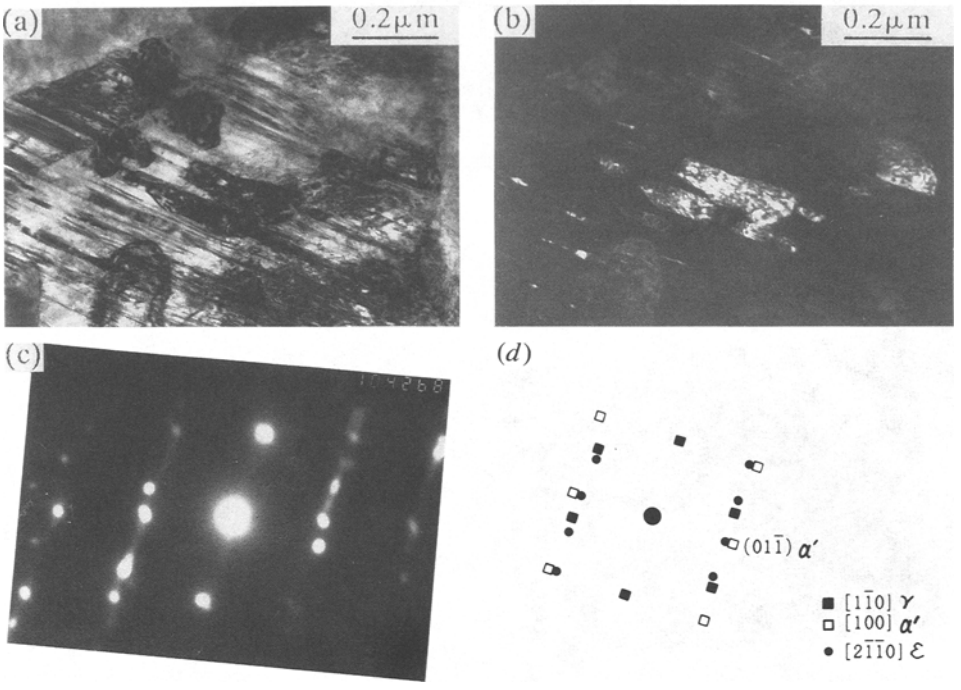

Fig. 11 — Partially transformed austenite in 650 °C, 1-h tempered specimen after 10 pct cold reduction: (*a*) bright-field image, (*b*) (011)α′ dark-field image, (*c*) selected area diffraction pattern from transformed area, and (*d*) index of (*c*).

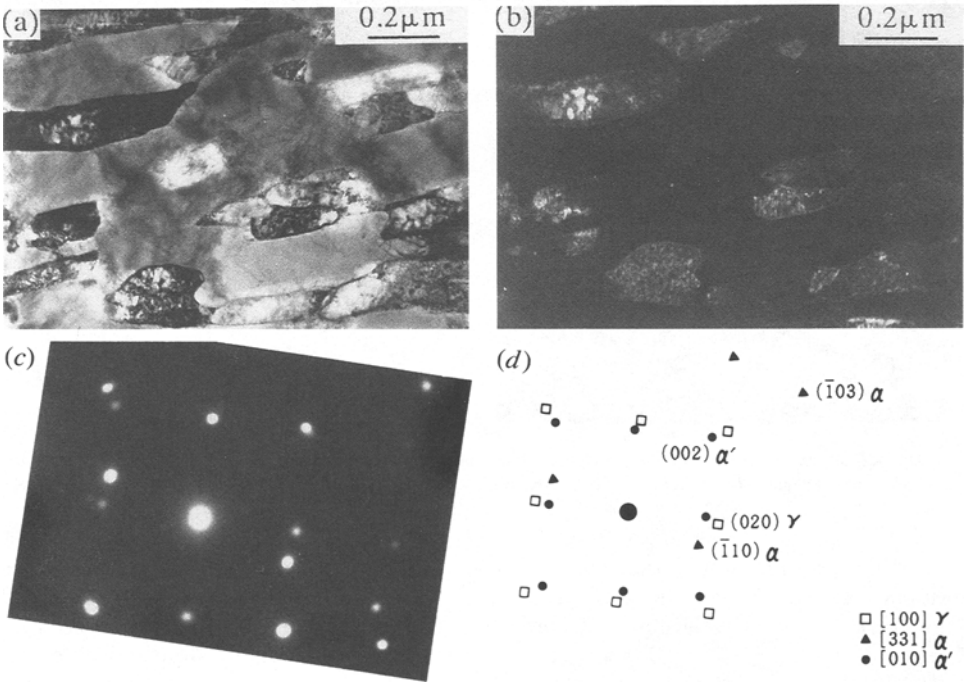

Fig. 12 — α′-martensite transformed from retained austenite after 50 pct cold reduction of 650 °C tempered alloy: (*a*) bright-field image, (*b*) (002)α′ dark-field image, (*c*) selected area diffraction pattern from transformed area, and (*d*) index of (*c*).

Table II. Volume Fraction of Austenite and ε-Martensite Phase before and after Tensile Deformation to Fracture at Room and Liquid Nitrogen Temperature

Specimen	Test Temperature (°C)	Before Test		After Test	
		γ	ε	γ	ε
2AT (550 °C/16 h)	RT*	36	0	28	3
	−196	36	0	16	6
2AT (650 °C/1 h)	RT*	54	6	14	2
	−196	52	6	00	0

*RT = room temperature.

particles generated a more localized type of dislocation structure and might, therefore, give a less detrimental effect on toughness. Moreover, the transformation of stable austenite will tend to occur very close to the crack tip, and interaction between the applied stress and the transformation-induced dislocations, which may even be beneficial to toughness, can be expected. It is proposed that this interaction will reduce the applied stress and, thereby, the stress intensity within a packet or lath.

The role of austenite precipitated during final tempering treatment was also crucial for the cryogenic toughness of Fe-13Mn-3Al steel. During ($\alpha + \gamma$) region tempering, the volume fraction of austenite increased with increasing tempering time and saturated to 36 pct after 16 hours at 550 °C, to 44 pct after 4 hours at 600 °C, and to 54 pct after 2 hours at 650 °C (Figure 5). The Charpy impact values (Figure 6) at liquid nitrogen temperature showed similar trends with the austenite volume fraction and showed saturated values after exactly the same tempering time needed for the saturation in austenite volume fraction. Figure 8 shows that the mechanical stability of austenite precipitated by tempering for various times is almost identical at each tempering temperature. Based on these results, we can conclude that as long as the mechanical stabilities are identical, an increased amount of austenite results in an increase in the cryogenic toughness of ferrite plus austenite steel. However, a great difference in cryogenic toughness was observed when the saturation impact values at each tempering temperature were compared. The saturation Charpy impact values at −196 °C were more than doubled from 105 to 220 J when tempering temperature was lowered from 650 °C to 550 °C. The mechanical stability of austenite at room and liquid nitrogen temperature after 550 °C tempering was superior to that of 650 °C tempered ones. The mechanical stability of austenite in 600 °C tempered specimens fell between that of these two austenites and so did the Charpy impact values at −196 °C. All of these results suggest that higher mechanical stability is essential for higher cryogenic toughness. The effect of mechanical stability far exceeds the effect of austenite volume fraction on the cryogenic toughness.

The stronger effect of mechanical stability than that of the volume fraction of austenite on the cryogenic toughness was also emphasized in ferritic 9Ni steel. However, the austenite formed in Fe-13Mn-3Al steel is mechanically far stabler than the austenite in 9Ni steel. The austenite formed during 550 °C tempering almost survived a 50 pct rolling reduction at room temperature, and about 40 pct of austenite remained untransformed after tensile fracture at liquid nitrogen temperature. Judging from this result, we can expect that, after tempering at 550 °C, austenite will withstand the plastic deformation in front of the crack tip and effectively blunt the propagation of cleavage cracks.

With larger austenite volume fractions than 9Ni steel, the cleavage impairment model by Morris and coworkers[5,29] may well apply for this alloy. The austenite transformed to new variants of martensite rotated around a $[011]\alpha//[111]\gamma$ axis by plastic deformation. The cleavage impairment model can well be applied in this case, but our results demonstrated that this model alone cannot sufficiently explain the toughness differences between 650 °C and 550 °C tempered alloy.

Another possible explanation for variations in cryogenic toughness is the differences in mechanical transformation products at liquid nitrogen temperature. In 650 °C tempered alloys, the austenite transformed to twin-related dislocated martensite, while in 550 °C tempered alloys, austenite transformed to ordinary dislocated martensite. The differences in martensite morphology are

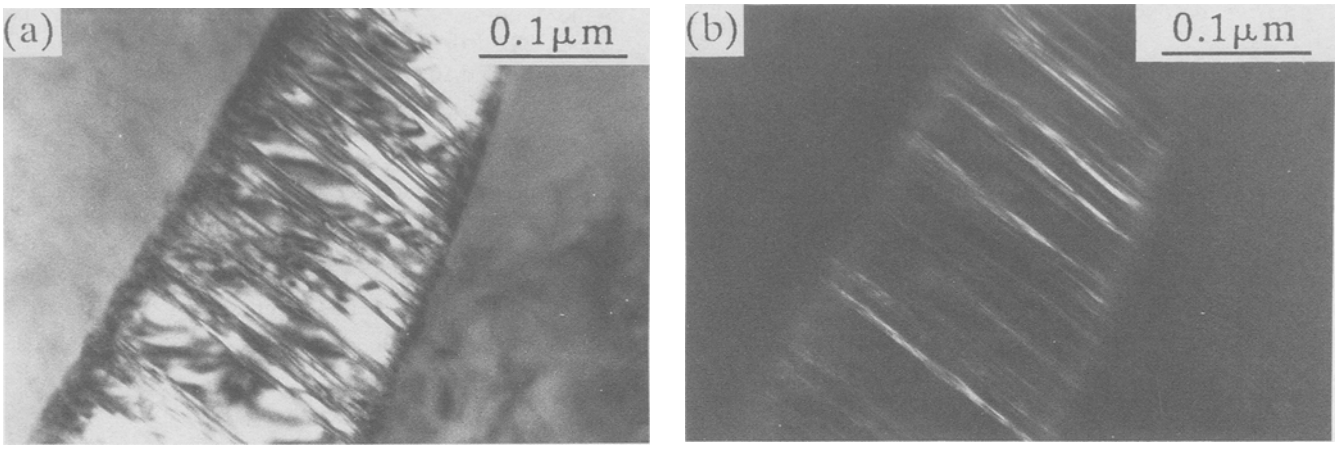

Fig. 13—ε-martensite transformed from austenite during tensile deformation of 550 °C tempered specimen at −196 °C: (*a*) bright-field image and (*b*) $(1\bar{1}00)\varepsilon$ dark-field image.

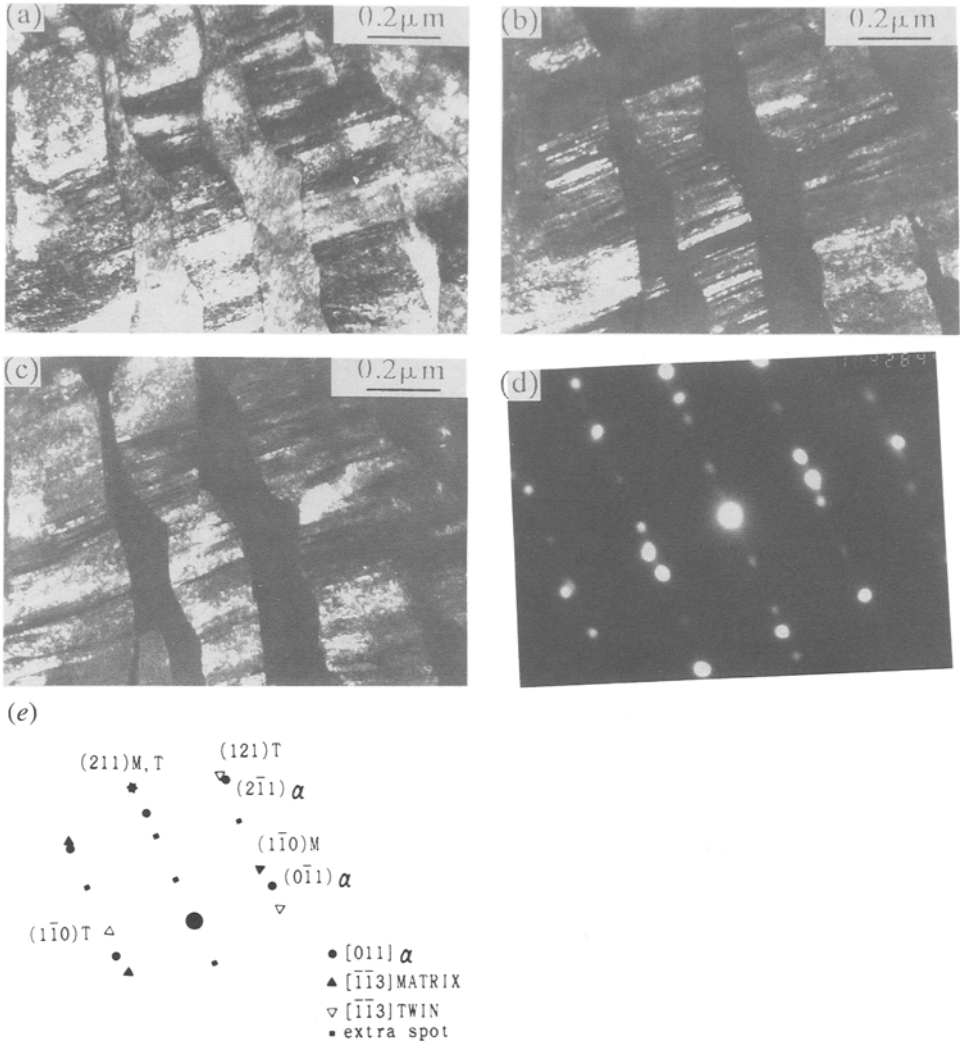

Fig. 14—Strain-induced twin-related lath martensite after tensile deformation of 650 °C tempered alloy at −196 °C: (*a*) bright-field image, (*b*) (1$\bar{1}$0) matrix dark-field image, (*c*) (1$\bar{1}$0) twin dark-field image, (*d*) selected area diffraction pattern, and (*e*) its index.

caused by the differences in stacking fault energy. The possibility there is that the fine-scale twin-related martensite can act like twins in internally twinned martensite and lower the ductility of this alloy.

V. SUMMARY

In Fe-13Mn-3Al steel, relatively large amounts of thermally stable austenite were precipitated after lower ($\alpha + \gamma$) region tempering. Measured maximum austenite volume fractions were 54, 44, and 36 pct after tempering at 650 °C, 600 °C and 550 °C, respectively. Mechanical stability of precipitated austenite greatly varied depending upon the final tempering temperature. At room temperature, austenite in 550 °C tempered specimens survived a 50 pct cold rolling, while 90 pct of them were transformed to lath martensite in 650 °C tempered ones. After tensile deformation to fracture at liquid nitrogen temperature, neither retained austenite nor ϵ-martensite was observed in 650 °C tempered specimens, while 16 pct austenite and 6 pct ϵ-martensite were presented in 550 °C tempered specimens. The mechanical stability of austenite was identified to be the key factor for the cryogenic toughness of this steel. Charpy impact values reached 220 J in 550 °C tempered specimens, while 105 J was obtained in 650 °C tempered specimen. The mechanical stability of austenite was not sensitive to tempering time at a constant temperature, and in this case, Charpy impact values increased with increased austenite volume fractions. Considering the outstanding mechanical stability and large volume fractions of austenite, the crack blunting model was proposed for improved cryogenic toughness in 550 °C tempered specimens. Another possible effect of the toughness of transformation products itself was suggested.

ACKNOWLEDGMENT

This research was supported by the Korea Ministry of Education through Grants for Advanced Materials Research 1989.

REFERENCES

1. S. Jin, J.W. Morris, Jr., and V.F. Zackay: *Metall. Trans. A*, 1975, vol. 6A, pp. 141-49.
2. S.K. Hwang, S. Jin, and J.W. Morris, Jr.: *Metall. Trans. A*, 1975, vol. 6A, pp. 2015-21.
3. C.K. Syn, S. Jin, and J.W. Morris, Jr.: *Metall. Trans. A*, 1976, vol. 7A, pp. 1827-32.
4. P. Pahuta, Z. Janik, L. Hyspecka, and K. Mazanec: *Trans. ISIJ*, 1986, vol. 26, pp. 649-54.
5. J.I. Kim, C.K. Syn, and J.W. Morris, Jr.: *Metall. Trans. A*, 1983, vol. 14A, pp. 93-103.
6. J.D. Bolton, E.R. Petty, and G.B. Allen: *Metall. Trans. A*, 1971, vol. 2A, pp. 2915-23.
7. M.J. Schanfein, M.J. Yokota, V.F. Zackay, E.R. Parker, and J.W. Morris, Jr.: ASTM STP 579, ASTM, Philadelphia, PA, 1975, pp. 361-77.
8. S.K. Hwang and J.W. Morris, Jr.: *Metall. Trans. A*, 1979, vol. 10A, pp. 545-55.
9. M. Niikura and J.W. Morris, Jr.: *Metall. Trans. A*, 1980, vol. 11A, pp. 1531-40.
10. S.W. Lee and H.-C. Lee: *Advan. Cryogenic Eng.*, 1990, vol. 36B, pp. 1347-54.
11. Z. Nishiyama: *Martensitic Transformation*, Academic Press, New York, NY, 1978, p. 49.
12. C.K. Syn, B. Fultz, and J.W. Morris, Jr.: *Metall. Trans. A*, 1978, vol. 9A, pp. 1635-40.
13. P.M. Kelly: *Acta Metall.*, 1965, vol. 13, pp. 635-46.
14. J.S. Bowles and J.K. Mackenzie: *Acta Metall.*, 1954, vol. 2, pp. 129-37.
15. H.M. Otte: *Acta Metall.*, 1957, vol. 5, pp. 614-27.
16. B. Cina: *J. Iron Steel Inst.*, 1954, vol. 177, pp. 406-22.
17. J.A. Venables: *Phil. Mag.*, 1962, vol. 7, pp. 35-44.
18. R. Lagneborg: *Acta Metall.*, 1964, vol. 12, pp. 823-43.
19. J.F. Breedis and W.D. Robertson: *Acta Metall.*, 1962, vol. 10, pp. 1077-88.
20. H. Schumann: *Arch. Eisenhuttenwes.*, 1969, vol. 40, pp. 1027-37.
21. L.I. Lysak, I.B. Goncharenko, and B.I. Nikolin: *Fiz. Metall. Metalloved.*, 1973, vol. 36 (1), pp. 97-101.
22. P.C.J. Gallagher: *Metall. Trans. A*, 1970, vol. 1A, pp. 2429-61.
23. T. Ericsson: *Acta Metall.*, 1966, vol. 14, pp. 853-65.
24. H.J. Rack and David Kalish: *Metall. Trans. A*, 1971, vol. 2A, pp. 3011-20.
25. C.N. Ahlquist: *Acta Metall.*, 1975, vol. 23, pp. 239-43.
26. H. Haga: *Trans. Iron Steel Inst. Jpn.*, 1973, vol. 13, pp. 141-44.
27. K.J. Kim and L.H. Schwartz: *Mater. Sci. Eng.*, 1978, vol. 33, pp. 5-20.
28. B. Fultz and J.W. Morris, Jr.: *Metall. Trans. A*, 1985, vol. 16A, pp. 2251-56.
29. D. Frear and J.W. Morris, Jr.: *Metall. Trans. A*, 1986, vol. 17A, pp. 243-52.
30. B. Fultz, J.I. Kim, Y.H. Kim, G.O. Fior, and J.W. Morris, Jr.: *Metall. Trans. A*, 1985, vol. 16A, pp. 2237-49.